Sensors and Materials, Vol. 31, No. 10 (2019) 3055–3066
MYU Tokyo

S & M 1992

Distinguishing Mass Loading Effect from Damping Loading Effect of Piezoelectric Immunosensor Using Energy Transfer Model

Yan Chen,[1*] Feng Tan,[2] and Wen Cao[1]

[1]Southwest University of Science and Technology, Mianyang 621010, China
[2]University of Electronic Science and Technology of China, Chengdu 611731, China

(Received June 30, 2019; accepted September 12, 2019)

Keywords: piezoelectric (PZ) immunosensor, energy transfer model (ETM), mass loading effect, damping loading effect, NuTu-19 IgG

For a piezoelectric (PZ) immunosensor operating under damping loading conditions, the mass loading and damping loading effects cannot be distinguished by frequency measurement alone. In this work, a special relationship between the vibrational amplitude on the surface of a quartz crystal and the viscosity and density product of the tested liquid is derived using the energy transfer model (ETM). To detect the NuTu-19 antibody concentration in immune serum, we simultaneously measure the resonant frequency and rectified load voltage of the PZ immunosensor. Excellent agreement is obtained between the ETM-calculated value and the actual value obtained by the Bradford method. The experimental results proved the correctness of the deduced equation and showed that the presented analytical method laid a foundation for further development of all types of quartz crystal sensors in the liquid phase.

1. Introduction

In recent years, the attention of many researchers in the fields of medicine and electronic information has been concentrated on piezoelectric (PZ) immunosensors. It is an ultrasensitive mass biosensor that combines the highly sensitive PZ effect of quartz crystals and the highly specific recognition of immunoreaction. The very small change in mass caused by antigen–antibody binding is identified by a corresponding change in the resonant frequency of the quartz crystal. Yang *et al.*[(1)] and Chen *et al.*[(2)] used PZ immunosensors to detect cervical and ovarian cancer in women; Montoya *et al.*[(3)] used them to detect tuberculosis; Pirinçci *et al.*[(4)] used them to detect ochratoxin A. Test results showed that in addition to some influencing factors, such as test temperature, humidity, and circuit jitter, there are still errors. These errors are sometimes large, and more severe cases can result in false positive rates. The reason for this is that the application is based only on the Sauerbrey theory.[(5)]

There are several points worth noting with respect to the accurate application of the Sauerbrey equation. First, the coating layer on the quartz surface must be thin and uniform

*Corresponding author: e-mail: ychen@swust.edu.cn
https://doi.org/10.18494/SAM.2019.2495

ISSN 0914-4935

with high rigidity.[6] However, the coatings, whether adhesive or bioactive substances, are viscoelastic films that give rise to a change in resonant frequency on account of their anelastic effect.[7,8] Therefore, if we blindly ascribe the total frequency variation of the PZ immunosensors to the change in mass on the surface of the quartz crystal, we will introduce analytic error.[9] Second, the mass attached to the quartz electrode surface is limited, usually less than 2% of the mass of quartz.[10] When the mass exceeds the tolerance, the quality factor of the resonator will drop sharply, significantly reducing the accuracy of measurement. Moreover, the resonator may even stop.[11] This poses a serious challenge to the operation of medical experiments. In addition, the application of gas-phase PZ sensing suffers from disadvantages, such as the tedious "dip and dry" process, and the on-line real-time data output analysis cannot be conducted.

Fortunately, the liquid-phase detection method using a PZ immunosensor can avoid the above disadvantages, but new problems are introduced. Martin *et al.*[12] pointed out that when a PZ sensor is operated in the liquid phase, both the mass loading and liquid damping loading effects can contribute to the change in resonant frequency. Therefore, it is impossible to distinguish the two different loading effects by frequency measurement alone. The modified Butterworth-Van Dyke model (M-BVD)[12] and quartz crystal microbalance-D (QCM-D)[13] are the two most common methods of analyzing the loading effects. Nevertheless, they are not practical. In the M-BVD model, both the dynamic resistance and the resonant frequency must be measured.[13,14] Since many component parts of the circuit have the equivalent impedance, the measurement is complicated. On the other hand, a small external interference easily interferes with the QCM-D method, resulting in inaccurate analysis results.

The goals of the present work are (i) to derive the explicit relationship between the vibration amplitude on the surface of quartz crystal and the viscosity and density product of the tested liquid using the energy transfer model (ETM), (ii) to detect NuTu-19 IgG from immune serum in the liquid phase by measuring both the resonant frequency and the vibration amplitude, and (iii) to distinguish the effect of mass loading from that of damping loading on a PZ immunosensor using the measured data.

2. Materials and Methods

2.1 Methods

2.1.1 Analysis of loading effect on PZ immunosensor using ETM

In the gas phase, the relationship between the changed mass and the corresponding changed frequency was shown by Sauerbrey[5] in 1959 as

$$\Delta f_m = -\frac{2nf_q^2}{\sqrt{\mu_q \rho_q}} \frac{\Delta m}{S}, \tag{1}$$

where Δm is the weight change on the surface quartz crystal, S is the area of the electrode surface, n is the overtone number, f_q is the fundamental frequency of the quartz crystal, μ_q is the shear modulus of quartz, ρ_q is the density of quartz, and Δf_m is the observed frequency shift caused by the mass loading effect.

In the liquid phase, the frequency change was described in terms of the viscosity and density product as[15]

$$\Delta f_L = -\frac{f_q^{\frac{3}{2}}}{\sqrt{\pi \mu_q \rho_q}} \sqrt{\rho_L \eta_L}, \tag{2}$$

where ρ_L and η_L are the density and absolute viscosity of the attached liquid, respectively, and Δf_L is the observed frequency shift caused by the liquid loading effect.

In fact, owing to the effect of the microstructure on the quartz electrode surface, the mass loading effect will also be caused by the deposited liquid film under certain conditions,[12] as shown by

$$\Delta f_{total} = \Delta f_m + \Delta f_L = -\left(\frac{2nf_q^2}{\sqrt{\mu_q \rho_q}} \frac{\Delta m}{A} + \frac{f_q^{\frac{3}{2}}}{\sqrt{\pi \mu_q \rho_q}} \sqrt{\rho_L \eta_L} \right), \tag{3}$$

where Δf_{total} is the measured total frequency shift. Therefore, the two different loading effects cannot be distinguished by the frequency testing theory alone in a liquid environment.

The main idea of the ETM is that the PZ resonator and deposited film form a compound resonator. When a foreign film is deposited on the surface of the quartz crystal, a portion of the energy stored in the unloaded resonator vibration system will be transferred to the film. The transferred energy will be shared between the stored and dissipated energies in accordance with the elastic and anelastic properties of the deposited film, respectively. It is assumed that the film deposited on the quartz surface does not have its own vibrational frequency, but vibrates synchronously with the quartz crystal surface with a frequency f_c[16] corresponding to that of the compound resonator.

Sauerbrey's experimental data led to the conclusion that the mass sensitivity depends on the vibrational amplitude distribution on the surface of the quartz crystal resonator. It has been stated that the mass sensitivity of a PZ immunosensor with a configuration of two identical circular and concentric electrodes follows a Gaussian-like distribution. Therefore, we assume that the vibrational amplitude distribution on the unloaded quartz resonator surface obeys

$$A(r) = A_0 \cos^2\left(\frac{\pi r}{2R_e} \right), \tag{4}$$

where A_0 is the maximum amplitude of vibration at the quartz resonator surface, R_e is the radius of the electrode, which is smaller than or equal to that of the quartz crystal, and r is the distance of a certain point on the quartz surface from the center of the plate. Furthermore, the vibrational amplitude of every point within the quartz resonator can be defined as[16,17]

$$A(r,y) = A_0 \sin\left(\frac{\pi y}{h_q}\right)\cos^2\left(\frac{\pi r}{2R_e}\right), \tag{5}$$

where $A_0 = A(0,\ h_q/2)$, $-h_q/2 \le y \le +h_q/2$, and h_q is the thickness of quartz. Then, the infinitesimal energy unit stored in an unloaded quartz crystal resonator is[18]

$$dE_q^s = \frac{1}{2}\omega_q^2 A^2(r,y)dm = \frac{1}{2}\rho_q\omega_q^2 A_0^2 \sin^2\left(\frac{\pi y}{h_q}\right)\cos^4\left(\frac{\pi r}{2R_e}\right)r dr\, d\phi\, dy, \tag{6}$$

where $0 \le \phi \le 2\pi$, $0 \le r \le R_e$. The stored vibrational energy of the unloaded quartz crystal resonator can be obtained as

$$E_q^s = \frac{1}{2}\rho_q h_q \omega_q^2 A_0^2 \pi {R_e}^2\left(\frac{3}{16} - \frac{1}{\pi^2}\right). \tag{7}$$

When a foreign film is deposited on the quartz resonator surface, in accordance with the main idea of the ETM, it vibrates synchronously with the quartz resonator surface at a new resonant frequency f_c. When the film is completely elastic, the amplitude of the resonator will not be affected by shear wave propagation. The vibrational amplitude within the adhesive film will be identical to that of the unloaded resonator, A_0. The energy transferred from the unloaded quartz resonator will be stored in the film, thus there is no energy loss. However, when the deposited film is anelastic, there is frictional force between adjacent cell layers. A portion of the transferred energy will be lost, resulting in the attenuation of the resonant amplitude, and the rest of the transferred energy will be stored in the film, maintaining its own vibration. In this case, the vibrational amplitude of the quartz surface is A_{1q}, and the vibrational amplitude of the deposited film can be expressed as

$$A_f(r,y) = A_{1q}\cos^2\left(\frac{\pi r}{2R_e}\right)\exp\left[-\left(\frac{\omega_c}{2\gamma_f}\right)^{\frac{1}{2}} y\right] = A_{1q}\cos^2\left(\frac{\pi r}{2R_e}\right)\exp\left[-\left(\frac{\omega_c}{2\gamma_f}\right)^{\frac{1}{2}} v_f t\right], \tag{8}$$

where $\gamma_f = \eta_f / \rho_f$ is the kinematic viscosity of the attached film and v_f is the velocity for a shear wave traveling in the anelastic film. The vibration amplitude of the compound resonator is shown in Fig. 1.

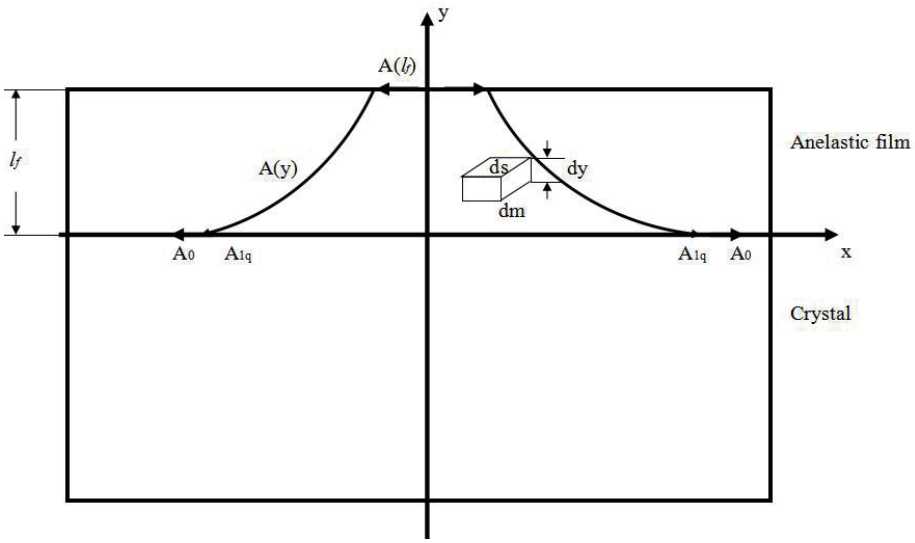

Fig. 1. Vibration amplitude of quartz-anelastic film.

The total vibrational energy dissipated by the anelastic film can be expressed as

$$E_f^d = \frac{1}{2}\rho_f \omega_c v_f A_{1q}^2 \pi R_e{}^2 \left(\frac{3}{16} - \frac{1}{\pi^2}\right) \times \left\{1 - \exp\left[-2\left(\frac{\omega_c}{2\gamma_f}\right)^{\frac{1}{2}} l_f\right]\right\}, \tag{9}$$

where l_f is the thickness of the anelastic film. Then, the rest of the energy of the quartz resonator is

$$E_{fq}^s = \frac{1}{2}\rho_q h_q \omega_c^2 A_{1q}^2 \pi R_e{}^2 \left(\frac{3}{16} - \frac{1}{\pi^2}\right). \tag{10}$$

At a constant frequency, we assume that the vibrational energy dissipated within the anelastic film will decrease the compound resonator vibrational amplitude; thus, from Eqs. (7), (9), and (10), we obtain

$$\begin{aligned} &\frac{1}{2}\rho_q h_q \omega_q^2 \pi R_e{}^2 \left(\frac{3}{16} - \frac{1}{\pi^2}\right)(A_0^2 - A_{1q}^2) \\ &= \frac{1}{2}\rho_f \omega_c v_f A_{1q}^2 \pi R_e{}^2 \left(\frac{3}{16} - \frac{1}{\pi^2}\right) \times \left\{1 - \exp\left[-2\left(\frac{\omega_c}{2\gamma_f}\right)^{\frac{1}{2}} l_f\right]\right\}. \end{aligned} \tag{11}$$

Furthermore, the shear wave velocity v_f can be determined from the acoustic impedance.[19,20]

$$\tilde{Z} = \left(\frac{\omega_c \rho_f \eta_f}{2} \right)^{\frac{1}{2}} (1 + j). \tag{12}$$

$$Z = \rho_f v_f . \tag{13}$$

Solving both Eqs. (12) and Eq. (13), we have

$$v_f = (\pi f_c)^{\frac{1}{2}} \left(\frac{\eta_f}{\rho_f} \right)^{\frac{1}{2}} . \tag{14}$$

Then, substituting $f_q = 1/2h_q \, (\mu_q/\rho_q)^{1/2}$, $\gamma_f = \eta_f / \rho_f$, and Eq. (14) into Eq. (11), we obtain

$$\begin{aligned} (\rho_f \eta_f)^{\frac{1}{2}} &= \frac{(\pi \rho_q \mu_q)^{\frac{1}{2}}}{f_c^{\frac{3}{2}} \left\{ 1 - \exp\left[-2 \left(\frac{\omega_c}{2\gamma_f} \right)^{\frac{1}{2}} l_f \right] \right\}} f_q \left(\frac{A_0^2}{A_{1q}^2} - 1 \right) \\ &= \frac{(\pi \rho_q \mu_q)^{\frac{1}{2}}}{f_c^{\frac{3}{2}} \left\{ 1 - \exp\left[-2 \left(\frac{\pi f_c \rho_f}{2\eta_f} \right)^{\frac{1}{2}} l_f \right] \right\}} f_q \left(\frac{A_0^2}{A_{1q}^2} - 1 \right). \end{aligned} \tag{15}$$

The exponent in Eq. (15) contains the reciprocal of the characteristic decay length δ, defined as

$$\delta = \left(\frac{\eta_f}{\pi f_c \rho_f} \right)^{\frac{1}{2}} . \tag{16}$$

Since the thickness of the anelastic film is far greater than the characteristic decay length, Eq. (15) can be simplified as

$$(\rho_f \eta_f)^{\frac{1}{2}} = \frac{\left(\pi \rho_q \mu_q \right)^{\frac{1}{2}}}{f_c^{\frac{3}{2}}} f_q \left(\frac{A_0^2}{A_{1q}^2} - 1 \right). \tag{17}$$

The equation explains the correlation between the product of viscosity and density of the anelastic film and the vibrational amplitude of the resonator surface. Therefore, the amplitude testing theory can be applied to measuring the damping loading effect on a PZ sensor in a damping environment.

2.1.2 Amplitude testing theory of quartz resonator

Because of the PZ effect, the relationship between the voltage across the quartz-resonator electrodes and the mechanical strain is shown as[17,21]

$$V = \frac{e}{\varepsilon}\left[1 - \cos\left(\frac{\pi f_c}{f_q}\right)\right] A_{1q}, \tag{18}$$

where e is the PZ constant and ε is the quartz permittivity. During testing, the rectified voltage can be used to represent the amplitude information. Thus, by applying both the amplitude and frequency testing theories, the two different loading effects can then be successfully differentiated by solving Eqs. (18), (17), (2), and (3) in turn.

2.2. Materials

To verify the correctness of the theoretical derivation, the concentration of NuTu-19 IgG in immune serum was tested and verified.

2.2.1 PZ immunosensor selection and preparation

Four 3rd-overtone AT-cut PZ sensors (10 MHz) were obtained from Tangshan Jing Yuan YuFeng Electronics Co., Ltd. (Hebei, China). Before use, all the sensors must be pretreated by a three-step process. First, the quartz crystals were mechanically cleaned with a cleaning agent and then with distilled water. Second, the quartz crystals were immersed in 1 mol/L sodium hydroxide solution for 10 min and then rinsed with distilled water. Lastly, the quartz crystals were immersed in 1 mol/L hydrogen chloride solution for 10 min, rinsed with deionized water (DW), and then dried in air.

2.2.2 NuTu-19 antigen and antibody preparation

NuTu-19, a rat ovarian cancer cell line, was purchased from American Type Culture Collection (Manassas, VA, USA) and cultured in accordance with the supplier's protocols. To obtain NuTu-19 IgG, inoculated rabbit heart blood was collected under light anesthesia one week after the last NuTu-19 cell injection. Then, serum IgG was separated using a protein separation column, and nonimmune rabbit serum was used as a negative control.

2.2.3 NuTu-19 antigen immobilization

NuTu-19 cells were cultured onto the surfaces of preprocessed quartz crystals in Dulbecco's modified Eagle medium (DMEM) (Gibco BRL, Grand Island, N.Y.) supplemented with 10% fetal bovine serum (Gibco BRL, Grand Island, N.Y.) and 100 μg/mL Amikacin. The cells were maintained in a humidified chamber at 37 °C in 5% CO_2 atmosphere. 36–48 h later, the number of cells reached maximum. Then, the quartz crystals were removed from the humidified chamber and dipped into 2% paraformaldehyde phosphate-buffered solution for 5 min to enhance cell immobilization.

2.2.4 Measurement procedure

To prevent the frequency stability from being affected by ambient temperature fluctuation, all tests were carried out in a thermostatic chamber at 25 °C. The resonance frequency f_0 of all preprocessed quartz crystals and the voltage U_0 of the unloaded QCM were first recorded. The quartz crystals on which NuTu-19 cells were immobilized were washed with PBS (pH 7.4) and DW, and then put in bovine serum albumin (BSA) (0.1 mg cm^{-3}) to reduce the interference from nonspecific adsorption. After thorough rinsing with PBS and DW, the crystals were dried at 25 °C, and the frequency f_1 and voltage U_1 were measured in the gas phase. Then, the serum-free NuTu-19 IgG was made to flow over the crystal surface through flow injection. When the frequency was stable, the frequency f_2 and voltage U_2 were detected under the liquid phase condition. Finally, the quartz crystals were covered with NuTu-19 IgG serum. When the reaction between the immobilized antigen and NuTu-19 IgG was complete, the steady-state resonant frequency f_3 was measured, and the steady-state voltage U_3 was also recorded under the liquid phase condition. Figure 2 shows that the target antibody is recognized by the NuTu-19 antigen on the electrode surface.

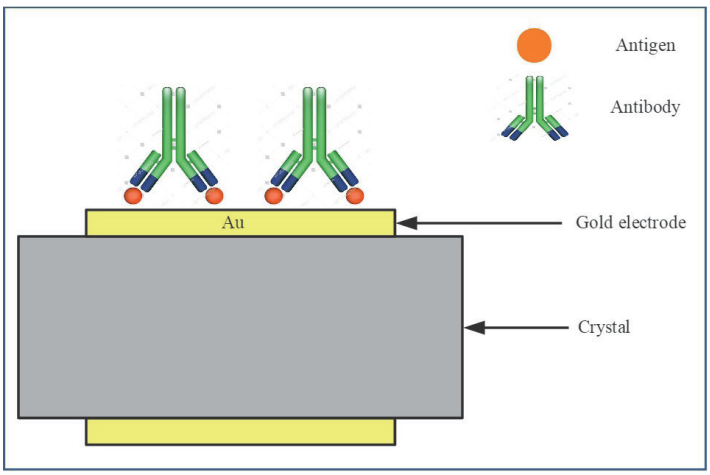

Fig. 2. (Color online) Reaction process of NuTu-19 antigen and NuTu-19 IgG.

3. Results and Discussion

3.1 Loading effect of antigen immobilization

Theoretically, the gas-phase testing was considered to reveal only the mass loading effect, but the ETM calculation results showed that although the analysis and quantification are carried out under the gas phase condition, NuTu-19 cell immobilization causes a relatively small damping loading effect, as shown in Table 1. The main reason for this is that the NuTu-19 cell membrane does not have strict rigidity with anelastic characteristics.

Figure 3 shows the frequency changes caused by NuTu-19 cell immobilization. Although the frequencies based on the Sauerbrey theory and those of the ETM were not the same, the error between the two methods can be ignored upon antigen immobilization. The main reason for this is that the two curves almost coincide, as shown in Fig. 3, indicating that the damping effect is relatively small. Therefore, the change in frequency can be considered a consequence of the changed mass of the NuTu-19 cell immobilization; in other words, the damping loading effect of the NuTu-19 cell film can be ignored in gas phase measurements.

3.2 Interaction

When the serum without NuTu-19 IgG was made to flow over the PZ sensor electrode surface, the resonator was markedly affected by liquid damping and its output amplitude

Table 1
Mass loading effect and damping loading effect on the surface of crystals caused by NuTu-19 cell immobilization.

Crystal	1#	2#	3#	4#
ΔU^1 (mV)	10	15	23	28
$\Delta f_{total}{}^1$ (Hz)	276	310	402	479
$\Delta f_m{}^1$ (Hz)	272	303	393	468
$\Delta f_L{}^1$ (Hz)	4	7	9	11

ΔU^1 is the changed voltage in the gas phase after NuTu-19 cell immobilization, $\Delta U^1 = U_1 - U_0$, $\Delta f_{total}{}^1$ is the measured total frequency shift in the gas phase after NuTu-19 cell immobilization, $\Delta f_{total}{}^1 = f_1 - f_0$, $\Delta f_m{}^1$ is the mass loading effect in the gas phase after NuTu-19 cell immobilization, and $\Delta f_L{}^1$ is the liquid loading effect in the gas phase after NuTu-19 cell immobilization.

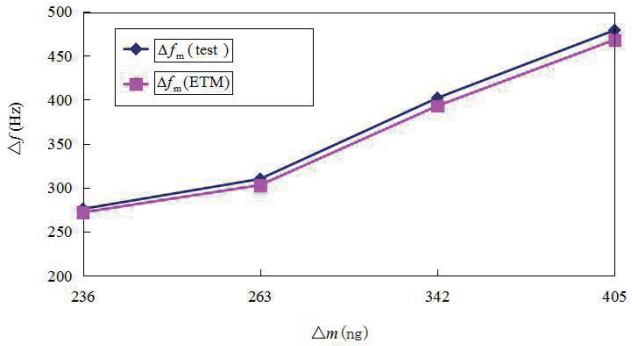

Fig. 3. (Color online) Changes in frequency caused by NuTu-19 cell immobilization.

dropped sharply. The change in voltage was around 960 mV, as shown in Table 2. The results of ETM calculation showed that there were slight frequency shifts caused by the mass loading effect. Fortunately, they were all no more than 2 Hz and within the error tolerance. Therefore, it can be considered that no immunoreaction occurred in the negative control group, and all the frequency changes resulted from the damping effect of the serum solution. In contrast, when the serum solution with NuTu-19 IgG was made to flow over the sensor electrode surface, the NuTu-19 antigen specifically combined with its target antibody. The deposited immunoreactants as the mass loading effect, resulted in a corresponding frequency shift. The dissipative properties of the immunoreactants also brought about a certain amount of frequency shift. The two different loading effects were differentiated by the ETM, as shown in Table 3.

3.3 NuTu-19 antibody concentration

The NuTu-19 IgG concentration was obtained on the basis of the Sauerbrey theory, ETM, and Bradford method. The error between the ETM-calculated value and the actual value was only 1% [(370 − 366)/370] × 100%, as shown in Fig. 4. However, the error between the

Table 2
Results for negative control.

Crystal	1#	2#	3#	4#
ΔU^2 (mV)	960	961	955	954
$\Delta f_{total}{}^2$ (Hz)	997	1000	999	1001
$\Delta f_m{}^2$ (Hz)	1.6	1.2	1	2
$\Delta f_L{}^2$ (Hz)	995.4	998.8	998	999

ΔU^2 is the changed voltage in nonimmune rabbit serum, $\Delta U^2 = U_2 - U_1$, $\Delta f_{total}{}^2$ is the measured total frequency shift in nonimmune rabbit serum, $\Delta f_{total}{}^2 = f_2 - f_1$, $\Delta f_m{}^2$ is the mass loading effect in nonimmune rabbit serum, and $\Delta f_L{}^2$ is the liquid loading effect in nonimmune rabbit serum.

Table 3
Results of NuTu-19 antibody test.

Crystal	1#	2#	3#	4#
ΔU^3 (mV)	200	289	275	315
$\Delta f_{total}{}^3$ (Hz)	351	423	511	608
$\Delta f_m{}^3$ (Hz)	264	290	384	457
$\Delta f_L{}^3$ (Hz)	87	133	127	151

ΔU^3 is the changed voltage in immune rabbit serum, $\Delta U^3 = U_3 - U_2$, $\Delta f_{total}{}^3$ is the measured total frequency shift in immune rabbit serum, $\Delta f_{total}{}^3 = f_3 - f_2$, $\Delta f_m{}^3$ is the mass loading effect in immune rabbit serum, and $\Delta f_L{}^3$ is the liquid loading effect in immune rabbit serum.

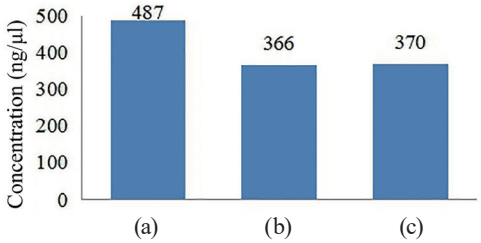

Fig. 4. (Color online) NuTu-19 IgG concentration: (a) value calculated on the basis of Sauerbrey theory, (b) ETM-calculated value, and (c) actual value (obtained by Bradford method).

value calculated on the basis of Sauerbrey theory and the actual value was beyond 30%. The comparison showed that the mass loading effect was distinguished from the damping loading effect on the PZ immunosensor using ETM, and that the detection accuracy was significantly improved.

4. Conclusions

A novel method of distinguishing the mass loading effect from the damping loading effect on a PZ immunosensor using the ETM is introduced in this paper. When the analysis and quantification are performed under the gas phase condition, a bioactivator is not strictly applicable to the rigid-layer behavior of a film fabricated by gas-phase mass deposition; thus, its dissipative effect must be considered. When the reaction and measurement are in the liquid phase, both effects must be considered. Using the ETM and frequency and amplitude testing theories, we succeeded in distinguishing the frequency shifts caused by the deposited immunoreactants from the total frequency variation of the PZ immunosensor, improving the detection accuracy significantly. Moreover, this new analytical method laid a foundation for further development of all types of quartz crystal sensors under the liquid phase.

Acknowledgments

We are grateful to Dr. H. S. Shi for his assistance in the experimental test and also to the State Key Laboratory of Biotherapy of Sichuan University for providing the biochemical experimental materials. This work was supported by the Dr. Foundation of Southwest University of Science and Technology (14zx7121).

Conflicts of Interest

The authors declare no conflicts of interest.

References

1 L. Yang, X. H. Huang, L. Sun, and L. Xub: Sens. Actuators, B **224** (2016) 863.
2 Y. Chen, X. H. Huang, and H. S. Shi: Asian Pac. J. Cancer Prev. **13** (2012) 3423.
3 A. Montoya, C. March, and Y. J. Montagu: Curr. Top. Med. Chem. **17** (2017) 1623.
4 Ş. Ş Pirinçci, Ö. Ertekin, D. E. Laguna, F. Ş. Özen, Z. Z. Öztürk, and S. Öztürk: Sensors **18** (2017) 1161.
5 G. Sauerbrey: Z. Phys. **155** (1959) 206.
6 R. L. Bunde, E. J. Jarvi, and J. J. Rosentreter: Talanta **46** (1998) 1223.
7 E. J. Calvo, R. Etchenique, and P. N. Bartlett: Faraday Discuss. **107** (1997) 141.
8 O. Wolff, E. Seydel, and D. Johannsmana: Faraday Discuss. **107** (1997) 91.
9 Y. H. Huang, J. Fu, and Z. M. Qiu: Chinese J. Electron. **36** (2008) 291.
10 C. S. Lu and A. W. Czanderna: Applications of Quartz Crystal Microbalances in Analytical Chemistry in Methods and Phenomena (Elsevier Publisher, London, 1984).
11 R. M. Mueller and W. White: Rev. Sci. Instrum. **39** (1968) 291.
12 S. J. Martin, V. Granstaff, and G. C. Frye: Anal. Chem. **63** (1991) 2272.
13 Y. G. Dong and G. P. Feng: Sens. Actuators, B **24** (1995) 62.
14 S. J. Martin, K. O. Wessendorf, and C. T. Geber: Measuring Liquid Properties with Smooth and Textured Surface Resonators (UFFC, Salt Lake City, 1993).

15 K. K. Kanazawa and J. G. Gordon: Anal. Chim. Acta **175** (1985) 99.
16 V. M. Mecea and R. V. Bucur: Thin Solid Films **60** (1979)73.
17 V. M. Mecca: Sens. Actuators, A **40** (1994) 1.
18 E. P. Feynman, R. B. Leighton, and M. Sands: The Feynman Lectures on Physics (Addison-Wesley, New Jersey, 1966).
19 M. S. Greenwood and J. A. Bamberger: Ultrasonics **39** (2002) 623.
20 L. Elvira, P. Resa, and P. Castro: Ultrasonics **53** (2013) 754.
21 E. Benes: J. Appl. Phys. **56** (1984) 608.